Optical and Quantum Electronics (2021) 53:518
https://doi.org/10.1007/s11082-021-03168-4

Figure of merit enhancement of surface plasmon resonance biosensor based on Talbot effect

Shahryar Farhadi[1] · Ali Farmani[1] · Abdolsamad Hamidi[1]

Received: 18 January 2021 / Accepted: 15 July 2021 / Published online: 14 August 2021

Abstract
This paper reports the numerical investigation of the Talbot effect for biomaterial detection at optical frequencies. Cytop polymer grating Plasmonics structure with periodicity comparable to the incident wavelength are applied to evaluate of the plasmonics Talbot biosensor. Significant sensitivity from the proposed Talbot biosensor is obtained. For this purpose, the effect of the different biomaterials including Ether, Ethyleneglycol, Chlorobenzene and Quinoline on plasmonics Talbot effects at wavelength range of 550-650 nm are then inspected to improve the structural parameters of the biosensor. Also, the sensitivity and figure-of-merit are calculated. Our numerical results show that the proposed biosensor are able to operate as a high sensitivity with maximum FOM of 20.99, and sensitivity of 324 nm/refractive index unit for small change of Δn= 0.4, in the refractive index of biomaterials. We believe that the proposed biosensor can be applied as a label free on-chip biosensor.

Keywords Surface Plasmon Resonance · Biosensor · Talbot effect

1 Introduction

When a monochromatic beam is propagated through a periodic structure such as grating platforms, the pattern of that configuration is provided to repeat itself occasionally with increasing distance of the pattern from the platform which known as Fresnel regime (Salama et al. 1999; Siegel et al. 2001; Wang et al. 2009). This distance is known as the Talbot distance, and fantastic effects may also be defined at this distances, where the multiple frequency self-imaging pattern can occur. This phenomena as a self-imaging pattern of the grating structure was introduced by H.F. Talbot in 1836, and has been the received remarkable attention from research groups in the field of atom optics and plasmonics (Podanchuk et al. 2014; Kovalenko et al. 2013; Zhang et al. 2009; Dennis et al. 2007). Therefore, various research groups have used talbot effect form practical applications in gratings and diffractive structure. Also, several optimized algorithms are proposed (Chen et al. 2020; Wang and Chen 2020; Xu et al. 2019; Zhao et al. 2019). As an example Li et al proposed

✉ Ali Farmani
farmani.a@lu.ac.ir

[1] School of Electrical and Computer Engineering, Lorestan University, Khoramabad, Iran

intelligence platform (Li et al. 2018). Wang et al proposed machine learning algorithm (Wang et al. 2017). And several related works are presented recently (Xia et al. 2017; Chen et al. 2016; Shen et al. 2016; Hu et al. 2015). This optimized algorithms have advanced applications (Xu and Chen 2014; Zhang et al. 2020, 2021; Zhao et al. 2021). Chen group work on bio-science with optimized algorithm (Tu et al. 2021; Shan et al. 2021; Yu et al. 2021; Hu et al. 2021; Zhao et al. 2014; Yu et al. 2020). The interest in this phenomena is not only theoretical aspect (Koriakovskii and Marchenko 1981; Liu et al. 2015). The Talbot effects as a remarkable phenomena of periodic structure have a advanced applications, such as switch, sensor, optical metrology, laser array illumination, detector and so on Feng et al. 2020; Fu and Yang 2020; Jiang et al. 2020,?. For example protein is a main components which is considered by research groups (Zhang and Liu 2019; Xu et al. 2020). Alzheimer detection is also so important (Zhu et al. 2020) and several sensing platforms (Zhu et al. 2020; Hu et al. 2020; Qu et al. 2019; Jiang et al. 2013; Wang et al. 2020; Zou et al. 2019). However, the self-imaging pattern is seen as the period of the structure is highly larger than the incident light beam, for the condition of resonant diffraction periodic structure whose period is relatively comparable to the incident frequency, the electric field profile at the repeated distance of the periodic structure will also revive periodically, called as the quasi-Talbot phenomena (Podanchuk et al. 2013, 2011, 2013, 2015; Iwata et al. 2011). In the year 2012, Hua research group developed Talbot effect beyond the paraxial limit at optical frequencies (Hua et al. 2012). In the year 2018, JINWOO group experimentally demonstrate a new design for passive Talbot amplification of repetitive optical waveforms (Jeon et al. 2018). In the year 2020, Aviad and co-worker focused on use of talbot effect in label free biosensors for therapeutic purpose. They proposed a label-free sensor on a chip, operating in near-infrared for monitoring of absorption line signatures based on molecular vibrations (Katiyi and Karabchevsky 2020). In the same year, X-ray measurements is introduced by Talbot effect by Brazhnikov research group. These proposed sensors able to detect a very small quantity of molecules (Brazhnikov et al. 2020).

In several practical applications, long grating structures are applied because of its good behavior, with periods ranging from several centimeter to higher than hundred of centimetres (Lin et al. 2020; Zuo et al. 2015, 2017; Zhang et al. 2020). However, there exist some advanced nano-applications in which small footprint displacements and exact contrast need to be calculated (Li et al. 2018, 2017; Wang et al. 2017; Xia et al. 2017). In typical, several applications based on the Talbot effect, cannot be used to nano-scale configuration with grating platforms comparable to the incident beam wavelength. Some numerical researches have focused on the self-image patterns in one-dimenssional structure the paraxial limit, and many of them differences in the self-image patterns were predicted. Also, these numerical results, always, have not been validated by experimental ones owing to their restriction in fabrication process.

Fortunately, in this years, by introducing the plasmonics fields, the Talbot effect was seen in naoscale structure (Wang et al. 2010; Li et al. 2011; Shi et al. 2015; Kim et al. 2020). However, the fast damping of surface waves in nobel metals restricted the investigate to only the first Talbot distance. Therefore, the new material such as polymers with high mobility features is needed (Kim et al. 2020). Despite remarkable practical investigations on biosensors based on talbot, there is still much researches to improve the overall performance of such biosensors.

In this work, we have analyzed the Talbot effect of polymer grating in the self-imaging pattern of Cytop polymer for biomaterial detections. We have numerically modeled the periodic structure with finite-difference time-domain (FDTD) as an Ether, Ethyleneglycol, Chlorobenzene and Quinoline biosensor. As expected, the Talbot effect appears. We have numerically found that the contrast of the self-images pattern changes as we harness the biomaterials. Also, a comparison of the previous results with the proposed model provided and shows that a changes of the contrast of the self-images pattern is due to the change of refractive index of biomaterial. Therefore, the proposed structure can be used as a highly sensitive biosensor.

The rest of this paper is organized as follows. In Sect. 2, the numerical structure of the Talbot biosensor is presented. Then, pivotal parameters of sensors are introduced. In the same Section, the main operation mechanism of proposed model is provided. In Sect. 3, by utilizing the different biomaterials, the Talbot effect for monitoring of the materials is applied. Moreover, obtained result compared with some previous works. Finally, the main conclusions in Sect. 4 is presented.

2 Proposed Talbot bioensor

2.1 Structure of the Talbot bioensor

Figure 1 presented the 3D-view of the proposed biosensor. As can be seen, the proposed plasmonics talbot biosensor is composed of a Cytop polymer grating layer for generating of talbot wave and air medium. The talbot structure is assumed to be illuminated by a tunable semiconductor laser in the range of 550 nm to 650 nm, and incident angle of θ is injected from left edge side. As a talbot biosensor, several biomaterials including Ether, Ethyleneglycol, Chlorobenzene and Quinoline are inspected. Schematic configuration of proposed sensor is depicted in Fig. 1. It consists of Cytop as substrate with grating period of Λ and duty cycle of 50 percent. The refractive index of polymer Cytop in range of 0.2 μm to 1.2 μm is shown in Fig. 2. The grooves are etched to depth of 0.5 μm. Other structural parameters of the device are tabulated in Table 1.

The main reason for choosing the talbot biosensor is that its simple and practical configuration with relatively compact footprint. The total footprint of the biosensor is 3.9 μm ×2.4 μm ×1.9 μm which is a very good candidate for portable platforms. It is worth to mentioning that the surface of injected biomaterial in the talbot biosensor has a grating configuration; therefore, it can be used for simultaneous biomaterials detection.

Fig. 1 The 3D-schematic of the talbot biosensor

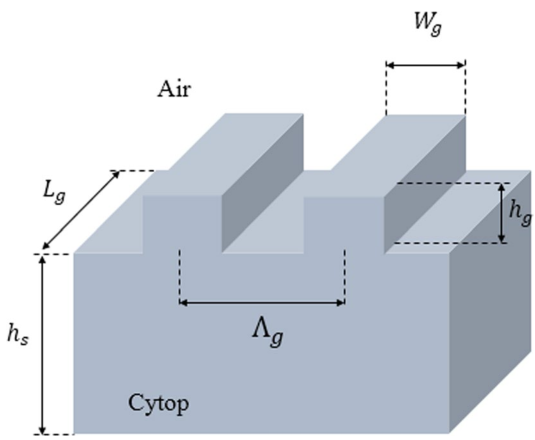

Table 1 The layers feature of the proposed Talbot biosensor

Parameter	Size
Λg	1.2 μm
W_g	0.6 μm
h_g	0.5 μm
L_g	1.9 μm
h_s	2 μm

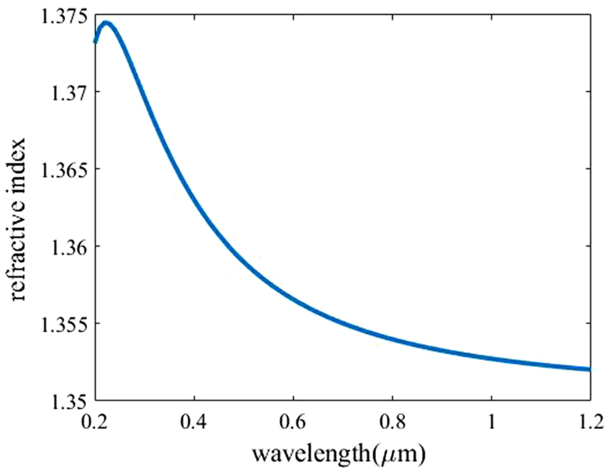

Fig. 2 The calculated of refractive index of polymer Cytop

Table 2 The refractive index of tested biomaterial as a function of wavelength

Parameters	$\lambda = 550nm$		$\lambda = 650nm$	
Ether	n = 1.3	n = 1.31	n = 1.33	n = 1.34
Ethyleneglycol	n = 1.4	n = 1.42	n = 1.44	n = 1.45
Chlorobenzene	n = 1.5	n = 1.51	n = 1.52	n = 1.53
Quin0line	n = 1.6	n = 1.63	n = 1.64	n = 1.65

For selecting the appropriate parameters such as previous works, optimized algorithm is considered (Zhang et al. 2019, 2020a, b, c, d, 2021). For example Yang group used classification for optimization of the structures (Yang et al. 2019; Zhang et al. 2021; Gong et al. 2019).

Incident light of plane wave has been applied along the z axis. The pattern of electric field interference of the structure with air background is shown in Fig. 3. For a diffraction grating the self-imaging pattern is repeated at a distance known Talbot plane, c:

$$c = (\lambda/n_r)(1 - \sqrt{1 - (\lambda/n_r\Lambda)_2}) \tag{1}$$

Where λ and n_r are the free space wavelength and background refractive index, respectively. To examine sensing operation of device, grooves were filled with different material as listed in Table 2. From Table 2 it can been seen that for different wavelength, refractive

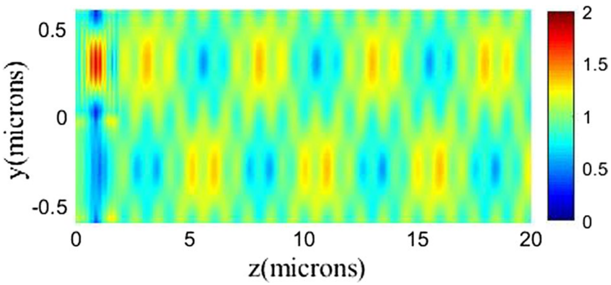

Fig. 3 The calculated of self-imaging pattern as the biomaterial is air

index of biomaterials change, and the self-imaging intensity pattern changes but the Talbot distance remains the same.

In next section, firstly, the crucial parameters of the biosensor is reviewed. Then, to gain a deep point of view about the mechanism of the structure several parameters are adjusted to find the appropriate results.

2.2 Talbot biosensor characteristics

To obtain deep point of view about talbot biosensor, potential results should be considered to detection of biomaterials including FoM, and sensitivity. In this regard, the sensitivity is expressed as:

$$S = \frac{\Delta\lambda}{\Delta n} \tag{2}$$

where $\Delta\lambda$ and Δn are respectively, reflection red-blue shifts and the biomaterial refractive index changes.

Also, figure of merit (FoM), as another main feature of the talbot biosensor, is calculated from:

$$FoM = [\frac{S}{FWHM} (1/RIU)] \tag{3}$$

where FWHM refers to the full width at half of the maximum parameter at the central wavelength.

In next section, firstly, it assume air condition for talbot biosensor with room temperature condition $T = 300°K$, and the incident wavelength of laser is tuned from $\lambda_0 = 550$ nm to λ_0=650 nm, and calculation is done by using FDTD package. Then, the effect of the different biomaterials including Ether, Ethyleneglycol, Chlorobenzene and Quinoline on the talbot reuslts are considered. Finally, to improve the calculated result, by considering best geometry of the talbot biosensor, highest sensitivity is calculated.

3 Result and discussion

To deep study the performance of the talbot biosensor, the FDTD method for detection of air is used. The electric field profile in this case is obtained in Fig. 3. In this case the temperature is 300 K. Here, the geometrical parameters are set as L_g= 1200 nm, w_g=

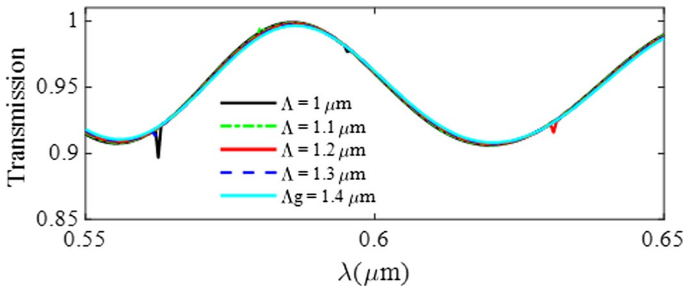

Fig. 4 The transmission spectra of structure for different Λ_s

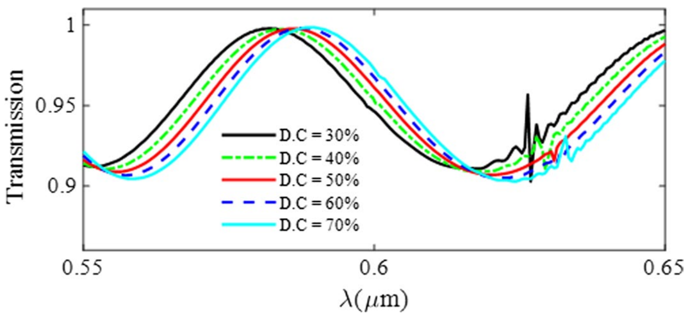

Fig. 5 The transmission spectra of structure for different D.Cs

500 nm, and n_{air}= 1 so that the talbot resonance wavelength is occurred around 550 nm. As can be seen, the self-imaging pattern is repeated with highly sensitivity and high contrast.

To further study the results of the proposed configuration, we have also investigated the effect of the Λ_s on the transmittance curve. As can be seen in Fig. 4, at resonance wavelength, the transmission variation by Λ_s is less than 0.1 and the throughput is greater than 0.9.

As D.C (Wg/Λ_g) is the another important parameter for evaluating the structure, this parameters is provided in Fig. 5. To discuss how the strong light-matter interaction between incident light and layer of Cytop and its effects on the sensing characteristics, we used different D.C of 30%, 40%, 50%, 60%, and 70% for transmission spectra, while keeping other parameters fixed. Figure 5 shows the transmission versus the resonance wavelength for different D.C. As can be seen, the variation of D.C leads to red and blue-shift of the transmission spectrum which is used for sensing mechanism.

To investigate how the length Lg affects the sensing properties, we tuned the Lg from 1.8 to 2 µm in steps of 0.05 µm, while keeping the other parameters fixed. Figure 6 illustrates the relationship between the transmission spectrum and the wavelength for different Lg. Figure 6 shows the red shift of the transmission can be used for sensing mechanism.

To exact study the effect of different biomaterials on the electric field profile, biomaterials are changed, whereas the other parameters are fixed. As illustrated in Fig. 7, different self-imaging pattern are produced for various biomaterials. In this case, easily several biomaterials can be detected.

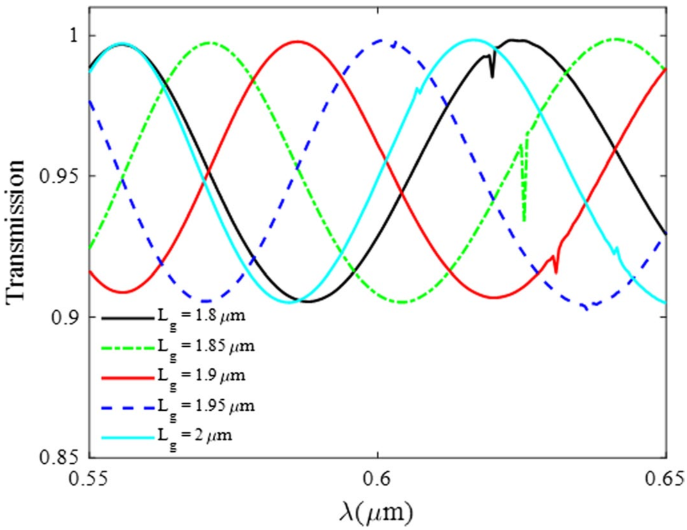

Fig. 6 The transmission spectra of structure for different Lg

The transmission spectra of sensor for different sensing materials is depicted in Fig. 8. The dip resonance frequency of device for air is about 525.2 nm. As it seen, by increasing the Δn the resonance frequency is red shifted.

Finally, we analyze the performance of parameters for different biomaterials including Ether, Ethyleneglycol, Chlorobenzene and Quinoline. The resonance frequency and relative sensitivity of talbot biosensor for each material is listed in Table 3.

As can be observed in Table 4, highest sensitivity of 324 nm/RIU by considering Chlorobenzene can be provided. Also, the highest FoM of 20.99 for Quinoline is obtained. The results are highly improved compared with previous works Farmani et al. 2018; Farmani 2019; Farmani and Mir 2019; Farmani et al. 2020; Hamzavi-Zarghani et al. 2019; Amoosoltani et al. 2019; Mozaffari and Farmani 2019; Farmani et al. 2020. Finally, by considering FDTD algorithm and the excitation of talbot waves, the performance of the talbot biosensor remarkably enhanced compared to the obtained results of the previous works provided in Table 4. As a result, the obtained results can be used in recent advanced applications Wang et al. 2017; Zhang et al. 2020, 2019; Sun et al. 2019.

4 Conclusion

Here, we have reported the model for a high sensitivity surface plasmon resonance biosensor for biomaterials detection, based on plasmonics Talbot effects. The performance of the biosensor was numerically studied with FDTD method. To evaluate of the biosensor different biomaterials including Ether, Ethyleneglycol, Chlorobenzene and Quinoline were also studied. It was observed that, for small variation of Δn= 0.4, in the biomaterials refractive index, FoM and sensitivity as high as 20.99 and 324nm/RIU are achievable in the biosensor, respectively. We envision that the proposed biosensor based on plasmonics Talbot effect can be used as a potential platform for on-chip biosensors.

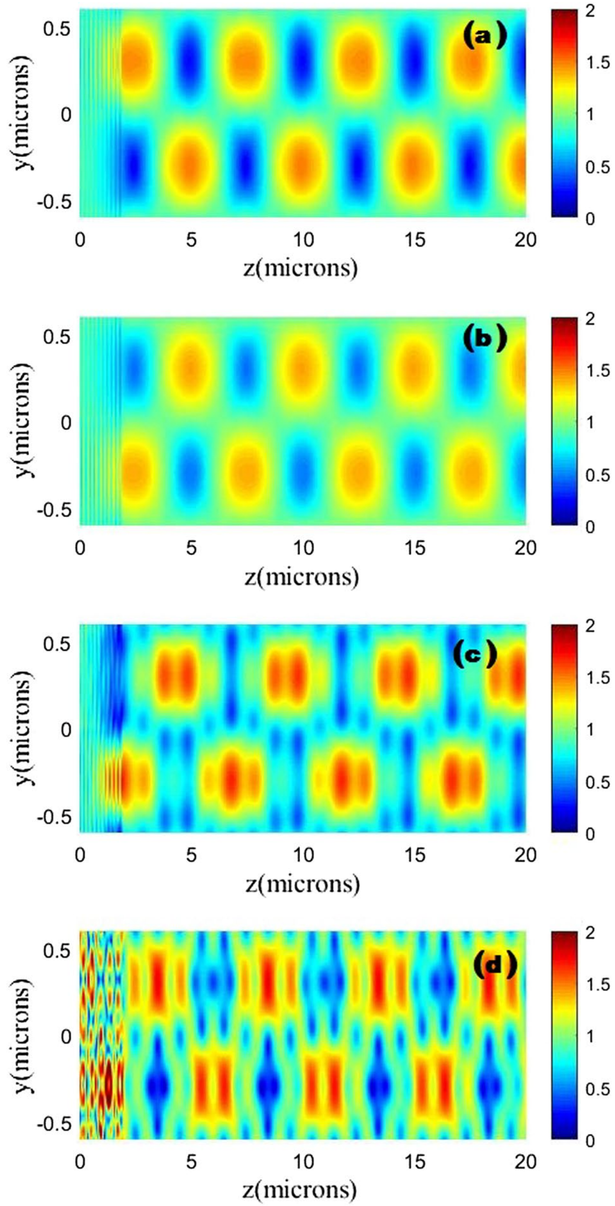

Fig. 7 The calculated of self-imaging pattern as the biomaterials are Ether, Ethyleneglycol, Chlorobenzene and Quinoline

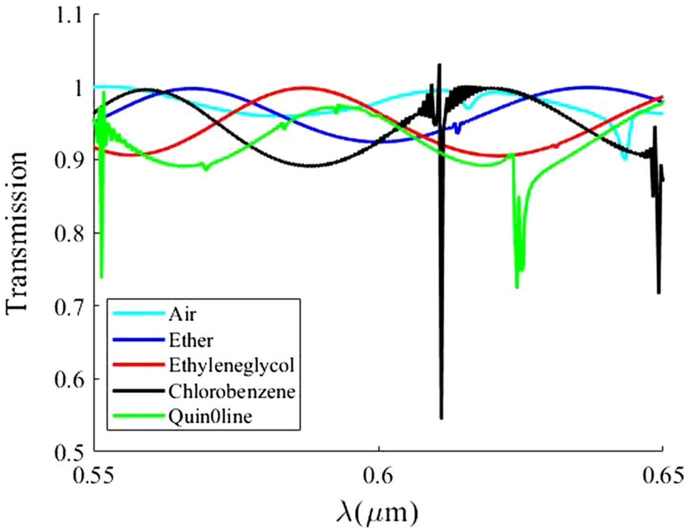

Fig. 8 The calculated of self-imaging pattern as the biomaterials are Ether, Ethyleneglycol, Chlorobenzene and Quinoline

Table 3 The calculated sensing parameters of the proposed structure

Material	λ_r	FWHM (nm)	S (nm/RIU)	FOM(RIU^{-1})
Air	525.2	17.3	–	–
Ether	537.8.2	18.7	42	2.24
Ethyleneglycol	556.2	17.3	184	9.15
Chlorobenzene	588.6	20.1	324	16.12
Quin0line	618.2	14.1	296	20.99

Table 4 Comparison of the sensing parameters of the present and previous works

References	FoM	S	Structure
Golfazani et al. (2020)	9.8	693.8	Metal-dielectric-metal Waveguide
Amoosoltani et al. (2020)	9	1500	Plasmonics Disk Resonators
Moradiani et al. (2020)	10	1271	PIT-like resonator
This Work	20.99	324	Plasmonics Cytop Polymer grating

Funding Information This research did not receive any specific grant from funding agencies.

Data Availability Statement All data included in this paper are available upon request by contact with the contact corresponding author.

Declaration

Conflict of interests The authors declare that they have no conflict of interest.

References

Amoosoltani, N., Yasrebi, N., Farmani, A., Zarifkar, A.: A plasmonic nano-biosensor based on two consecutive disk resonators and unidirectional reflectionless propagation effect. IEEE Sensors J. (2020)

Amoosoltani, N., Zarifkar, A., Farmani, A.: Particle swarm optimization and finite-difference time-domain (PSO/FDTD) algorithms for a surface plasmon resonance-based gas sensor. J. Comput. Electron. **18**(4), 1354 (2019)

Brazhnikov, D., Kotov, M., Kovalenko, A.: Reference-free wave-front sensor based on the Talbot effect, in *Fourteenth International Conference on Correlation Optics*, vol. 11369 (International Society for Optics and Photonics, 2020), vol. 11369, p. 113690X

Chen, H.L., Wang, G., Ma, C., Cai, Z.N., Liu, W.B., Wang, S.J.: An efficient hybrid kernel extreme learning machine approach for early diagnosis of Parkinson's disease. Neurocomputing **184**, 131 (2016)

Chen, H., Heidari, A.A., Chen, H., Wang, M., Pan, Z., Gandomi, A.H.: Multi-population differential evolution-assisted Harris hawks optimization: Framework and case studies. Futur. Gener. Comput. Syst. **111**, 175 (2020)

Dennis, M.R., Zheludev, N.I., de Abajo, F.J.G.: The plasmon Talbot effect. Opt. Express **15**(15), 9692 (2007)

Farmani, A., Soroosh, M., Mozaffari, M.H., Daghooghi,T.: Optical nanosensors for cancer and virus detections. In: Nanosensors for Smart Cities, pp. 419–432. Elsevier (2020)

Farmani, A.: Three-dimensional FDTD analysis of a nanostructured plasmonic sensor in the near-infrared range. JOSA B **36**(2), 401 (2019)

Farmani, A., Mir, A.: Graphene sensor based on surface plasmon resonance for optical scanning. IEEE Photon. Technol. Lett. **31**(8), 643 (2019)

Farmani, A., Mir, A., Bazgir, M., Zarrabi, F.B.: Highly sensitive nano-scale plasmonic biosensor utilizing Fano resonance metasurface in THz range: numerical study. Physica E **104**, 233 (2018)

Farmani, H., Farmani, A., Biglari, Z.: A label-free graphene-based nanosensor using surface plasmon resonance for biomaterials detection. Physica E **116**, 113730 (2020)

Feng, Q., Li, Y., Wang, N., Hao, Y., Chang, J., Wang, Z., Zhang, X., Zhang, Z., Wang, L.: A biomimetic nanogenerator of reactive nitrogen species based on battlefield transfer strategy for enhanced immunotherapy. Small **16**(25), 2002138 (2020)

Fu, X., Yang, Y.: Modeling and analysis of cascading node-link failures in multi-sink wireless sensor networks. Reliab. Eng. Syst. Saf. **197**, 106815 (2020)

Golfazani, A.J., Alipour, A., Bakhshipour, M., Farmani, A., Mir, A.: Analytical and numerical models of a highly sensitive MDM plasmonic nano-structure in near-infrared range. Plasmonics 1–6 (2020)

Gong, C., Hu, Y., Gao, J., Wang, Y., Yan, L.: An improved delay-suppressed sliding-mode observer for sensorless vector-controlled PMSM. IEEE Trans. Industr. Electron. **67**(7), 5913 (2019)

Hamzavi-Zarghani, Z., Yahaghi, A., Matekovits, L., Farmani, A.: Tunable mantle cloaking utilizing graphene metasurface for terahertz sensing applications. Opt. Express **27**(24), 34824 (2019)

Hu, J.w., Zheng, B.y., Wang, C., Zhao, C.h., Hou, X.l., Pan, Q., Xu, Z.: A survey on multi-sensor fusion based obstacle detection for intelligent ground vehicles in off-road environments. Front. Inf. Technol. Electron. Eng. **21**, 675 (2020)

Hu, L., Hong, G., Ma, J., Wang, X., Chen, H.: An efficient machine learning approach for diagnosis of paraquat-poisoned patients. Comput. Biol. Med. **59**, 116 (2015)

Hu, J., Chen, H., Heidari, A.A., Wang, M., Zhang, X., Chen, Y., Pan, Z.: Orthogonal learning covariance matrix for defects of grey wolf optimizer: insights, balance, diversity, and feature selection. Knowl.-Based Syst. **213**, 106684 (2021)

Hua, Y., Suh, J.Y., Zhou, W., Huntington, M.D., Odom, T.W.: Talbot effect beyond the paraxial limit at optical frequencies. Opt. Express **20**(13), 14284 (2012)

Iwata, K., Satoh, K., Moriwaki, K.: Compact sensor for measuring two-dimensional tilt using a two-dimensional transmission grating and the Talbot effect. Appl. Opt. **50**(3), 261 (2011)

Jeon, J., Maram, R., van Howe, J., Azaña, J.: Programmable passive Talbot optical waveform amplifier. Opt. Express **26**(6), 6872 (2018)

Jiang, Q., Wang, G., Jin, S., Li, Y., Wang, Y.: Predicting human microRNA-disease associations based on support vector machine. Int. J. Data Min. Bioinform. **8**(3), 282 (2013)

Jiang, D., Chen, F.X., Zhou, H., Lu, Y.Y., Tan, H., Yu, S.J., Yuan, J., Liu, H., Meng, W., Jin, Z.B.: Bioenergetic crosstalk between mesenchymal stem cells and various ocular cells through the intercellular trafficking of mitochondria. Theranostics **10**(16), 7260 (2020)

Katiyi, A., Karabchevsky, A.: Deflected Talbot mediated overtone spectroscopy in near-infrared as a label-free sensor on a chip, ACS sensors (2020)

Kim, G.W., Kang, S.H., Ha, J.W.: Characterizing the non-paraxial Talbot effect of two-dimensional periodic arrays of plasmonic gold nanodisks by differential interference contrast microscopy. Analyst **145**(23), 7541 (2020)

Koriakovskii, A., Marchenko, V.: A wave-front sensor based on the Talbot effect. ZhTFi **51**, 1432 (1981)

Kovalenko, A.V., Kotov, M.M., Kurashov, V.N., Movchan, M.M.: Role of diffraction grating profile in the wavefront sensor based on the Talbot effect. In: Eleventh International Conference on Correlation Optics, vol. 9066 (International Society for Optics and Photonics, 2013), vol. 9066, p. 90660R

Li, L., Fu, Y., Wu, H., Zheng, L., Zhang, H., Lu, Z., Sun, Q., Yu, W.: The Talbot effect of plasmonic nanolenses. Opt. Express **19**(20), 19365 (2011)

Li, K., Xia, F., Wang, M., Sun, P., Liu, T., Hu, W., Kong, W., Yun, M., Dong, L.: Discrete Talbot effect in dielectric graphene plasmonic waveguide arrays. Carbon **118**, 192 (2017)

Li, C., Hou, L., Sharma, B.Y., Li, H., Chen, C., Li, Y., Zhao, X., Huang, H., Cai, Z., Chen, H.: Developing a new intelligent system for the diagnosis of tuberculous pleural effusion. Comput. Methods Prog. Biomed. **153**, 211 (2018)

Lin, J., Cai, X., Liu, Z., Liu, N., Xie, M., Zhou, B., Wang, H., Guo, Z.: Anti-liquid-interfering and bacterially antiadhesive strategy for highly stretchable and ultrasensitive strain sensors based on Cassie-Baxter wetting state. Adv. Func. Mater. **30**(23), 2000398 (2020)

Liu, J., Zhou, S., Hu, S., Gao, H., He, Y., Cheng, Y.: Spectrum-integral Talbot effect for UV photolithography with extended DOF. IEEE Photon. Technol. Lett. **27**(20), 2201 (2015)

Moradiani, F., Farmani, A., Mozaffari, M.H., Seifouri, M., Abedi, K.: Systematic engineering of a nanostructure plasmonic sensing platform for ultrasensitive biomaterial detection. Opt. Commun. 126178 (2020)

Mozaffari, M.H., Farmani, A.: On-chip single-mode optofluidic microresonator dye laser sensor. IEEE Sens. J. **20**(7), 3556 (2019)

Podanchuk, D.V., Goloborodko, A.A., Kotov, M.M.: Features of the wavefront sensor based on the Talbot effect. In: 2013 International Conference on Advanced Optoelectronics and Lasers (CAOL 2013) (IEEE, 2013), pp. 337–339

Podanchuk, D.V., Kotov, M.M., Goloborodko, A.A., Kurashov, V.N., Dan'ko, V.P., Kurashov, A.V.: Influence of aperture size on wavefront sensor based on the Talbot effect in *Eleventh International Conference on Correlation Optics*, vol. 9066 (International Society for Optics and Photonics, 2013), vol. 9066, p. 90660S

Podanchuk, D.V., Kurashov, V.N., Goloborodko, A.A., Dan'ko, V.P., Kotov, M.M., Parhomenko, O.O.: Holographic wavefront sensor based on the Talbot effect. In: Tenth International Conference on Correlation Optics, vol. 8338 (International Society for Optics and Photonics, 2011), vol. 8338, p. 83380G

Podanchuk, D.V., Kurashov, V.N., Kovalenko, A.V., Dan'ko, V.P., Kotov, M.M., Goloborodko,N.S.: Adaptive wavefront sensor based on the Talbot effect, in *Twelfth International Conference on Correlation Optics*, vol. 9809 (International Society for Optics and Photonics, 2015), vol. 9809, p. 98090A

Podanchuk, D., Kovalenko, A., Kurashov, V., Kotov, M., Goloborodko, A., Danko, V.: Bottlenecks of the wavefront sensor based on the Talbot effect. Appl. Opt. **53**(10), B223 (2014)

Qu, K., Wei, L., Zou, Q.: A review of DNA-binding proteins prediction methods. Curr. Bioinform. **14**(3), 246 (2019)

Salama, N.H., Patrignani, D., De Pasquale, L., Sicre, E.E.: Wavefront sensor using the Talbot effect. Opt. Laser Technol. **31**(4), 269 (1999)

Shan, W., Qiao, Z., Heidari, A.A., Chen, H., Turabieh, H., Teng, Y.: Knowledge-based double adaptive weights for stabilization of moth flame optimizer: balance analysis, engineering cases, and medical diagnosis. Systems **214**, 106728 (2021)

Shen, L., Chen, H., Yu, Z., Kang, W., Zhang, B., Li, H., Yang, B., Liu, D.: Evolving support vector machines using fruit fly optimization for medical data classification. Knowl.-Based Syst. **96**, 61 (2016)

Shi, X., Yang, W., Xing, H., Chen, X.: Discrete plasmonic Talbot effect in finite metal waveguide arrays. Opt. Lett. **40**(8), 1635 (2015)

Siegel, C., Loewenthal, F., Balmer, J.: A wavefront sensor based on the fractional Talbot effect. Opt. Commun. **194**(4–6), 265 (2001)

Sun, M., Yan, L., Zhang, L., Song, L., Guo, J., Zhang, H.: New insights into the rapid formation of initial membrane fouling after in-situ cleaning in a membrane bioreactor. Process Biochem. **78**, 108 (2019)

Tu, J., Chen, H., Liu, J., Heidari, A.A., Zhang, X., Wang, M., Ruby, R., Pham, Q.V.: Evolutionary biogeography-based whale optimization methods with communication structure: towards measuring the balance. Knowl.-Based Syst. **212**, 106642 (2021)
Wang, M., Chen, H.: Chaotic multi-swarm whale optimizer boosted support vector machine for medical diagnosis. Appl. Soft Comput. **88**, 105946 (2020)
Wang, A., Gill, P., Molnar, A.: Light field image sensors based on the Talbot effect. Appl. Opt. **48**(31), 5897 (2009)
Wang, Y., Zhou, K., Zhang, X., Yang, K., Wang, Y., Song, Y., Liu, S.: Discrete plasmonic Talbot effect in subwavelength metal waveguide arrays. Opt. Lett. **35**(5), 685 (2010)
Wang, M., Chen, H., Yang, B., Zhao, X., Hu, L., Cai, Z., Huang, H., Tong, C.: Toward an optimal kernel extreme learning machine using a chaotic moth-flame optimization strategy with applications in medical diagnoses. Neurocomputing **267**, 69 (2017)
Wang, B., Zou, F., Cheng, J., Zhong, S.: Fault detection filter design for continuous-time nonlinear Markovian jump systems with mode-dependent delay and time-varying transition probabilities. Adv. Differ. Equ. **2017**(1), 1 (2017)
Wang, X.F., Gao, P., Liu, Y.F., Li, H.F., Lu, F.: Predicting thermophilic proteins by machine learning. Curr. Bioinform. **15**(5), 493 (2020)
Xia, J., Chen, H., Li, Q., Zhou, M., Chen, L., Cai, Z., Fang, Y., Zhou, H.: Computer ultrasound-based differentiation of malignant and benign thyroid nodules: an extreme learning machine approach. Methods Prog. Biomed. **147**, 37 (2017)
Xu, X., Chen, H.l.:Adaptive computational chemotaxis based on field in bacterial foraging optimization, Soft Computing **18**(4), 797 (2014)
Xu, L., Jiang, S., Zou, Q.: An in silico approach to identification, categorization and prediction of nucleic acid binding proteins, bioRxiv (2020)
Xu, Y., Chen, H., Luo, J., Zhang, Q., Jiao, S., Zhang, X.: Enhanced Moth-flame optimizer with mutation strategy for global optimization. Inf. Sci. **492**, 181 (2019)
Yang, Y., Hou, C., Lang, Y., Sakamoto, T., He, Y., Xiang, W.: Omnidirectional motion classification with monostatic radar system using micro-Doppler signatures. IEEE Trans. Geosci. Remote Sens. **58**(5), 3574 (2019)
Yu, C., Chen, M., Cheng, K., Zhao, X., Ma, C., Kuang, F., Chen,H.: SGOA: annealing-behaved grasshopper optimizer for global tasks. Eng. Comput. 1–28 (2021)
Yu, H., Li, W., Chen, C., Liang, J., Gui, W., Wang, M., Chen, H.: Dynamic Gaussian bare-bones fruit fly optimizers with abandonment mechanism: method and analysis. Eng. Comput. 1–29 (2020)
Zhang, X., Fan, M., Wang, D., Zhou, P., Tao, D.: Top-k feature selection framework using robust 0-1 integer programming. IEEE Trans. Neural Netw. Learn. Syst. (2020)
Zhang, X., Jiang, R., Wang, T., Wang, J.: Recursive neural network for video deblurring. IEEE Trans. Circuits Syst. Video Technol. (2020)
Zhang, Y., Liu, R., Wang, X., Chen, H., Li, C.: Boosted binary Harris hawks optimizer and feature selection. Eng. Comput. **1–30**,(2020)
Zhang, X., Wang, T., Luo, W., Huang, P.: Multi-level fusion and attention-guided CNN for image dehazing. IEEE Trans. Circuits Syst. Video Technol. (2020)
Zhang, K., Zhang, J., Ma, X., Yao, C., Zhang, L., Yang, Y., Wang, J., Yao, J., Zhao, H.: History matching of naturally fractured reservoirs using a deep sparse autoencoder. SPE J. 1–22 (2021)
Zhang, J., Liu, B.: A review on the recent developments of sequence-based protein feature extraction methods. Curr. Bioinform. **14**(3), 190 (2019)
Zhang, W., Zhao, C., Wang, J., Zhang, J.: An experimental study of the plasmonic Talbot effect. Opt. Express **17**(22), 19757 (2009)
Zhang, X., Wang, D., Zhou, Z., Ma, Y.: Robust low-rank tensor recovery with rectification and alignment. IEEE Trans. Pattern Anal. Mach. Intell. **43**(1), 238 (2019)
Zhang, H., Sun, M., Song, L., Guo, J., Zhang, L.: Fate of NaClO and membrane foulants during in-situ cleaning of membrane bioreactors: Combined effect on thermodynamic properties of sludge. Biochem. Eng. J. **147**, 146 (2019)
Zhang, J., Chen, Q., Sun, J., Tian, L., Zuo, C.: On a universal solution to the transport-of-intensity equation. Opt. Lett. **45**(13), 3649 (2020)
Zhang, X., Wang, T., Wang, J., Tang, G., Zhao, L.: Pyramid channel-based feature attention network for image dehazing. Comput. Vis. Image Underst. **197**, 103003 (2020)
Zhang, H., Guan, W., Zhang, L., Guan, X., Wang, S.: Degradation of an Organic Dye by Bisulfite Catalytically Activated with Iron Manganese Oxides: The Role of Superoxide Radicals. ACS Omega **5**(29), 18007 (2020)

Zhang, Y., Liu, R., Heidari, A.A., Wang, X., Chen, Y., Wang, M., Chen, H.: Towards augmented kernel extreme learning models for bankruptcy prediction: algorithmic behavior and comprehensive analysis. Neurocomputing **430**, 185 (2021)

Zhang, X., Wang, J., Wang, T., Jiang, R., Xu, J., Zhao, L.: Robust feature learning for adversarial defense via hierarchical feature alignment. Inf. Sci. **560**, 256 (2021)

Zhao, X., Li, D., Yang, B., Ma, C., Zhu, Y., Chen, H.: Feature selection based on improved ant colony optimization for online detection of foreign fiber in cotton. Appl. Soft Comput. **24**, 585 (2014)

Zhao, X., Zhang, X., Cai, Z., Tian, X., Wang, X., Huang, Y., Chen, H., Hu, L.: Chaos enhanced grey wolf optimization wrapped ELM for diagnosis of paraquat-poisoned patients. Comput. Biol. Chem. **78**, 481 (2019)

Zhao, D., Liu, L., Yu, F., Heidari, A.A., Wang, M., Liang, G., Muhammad, K., Chen, H.: Chaotic random spare ant colony optimization for multi-threshold image segmentation of 2D Kapur entropy. Knowl.-Based Syst. **216**, 106510 (2021)

Zhu, S., Wang, X., Zheng, Z., Zhao, X.E., Bai, Y., Liu, H.: Synchronous measuring of triptolide changes in rat brain and blood and its application to a comparative pharmacokinetic study in normal and Alzheimer's disease rats. J. Pharm. Biomed. Anal.s **185**, 113263 (2020)

Zhu, S., Zheng, Z., Peng, H., Sun, J., Zhao, X.E., Liu, H.: Quadruplex stable isotope derivatization strategy for the determination of panaxadiol and panaxatriol in foodstuffs and medicinal materials using ultra high performance liquid chromatography tandem mass spectrometry. J. Chromatogr. A **1616**, 460794 (2020)

Zou, Q., Xing, P., Wei, L., Liu, B.: Gene2vec: gene subsequence embedding for prediction of mammalian N6-methyladenosine sites from mRNA. RNA **25**(2), 205 (2019)

Zuo, C., Chen, Q., Tian, L., Waller, L., Asundi, A.: Transport of intensity phase retrieval and computational imaging for partially coherent fields: The phase space perspective. Opt. Lasers Eng. **71**, 20 (2015)

Zuo, C., Sun, J., Li, J., Zhang, J., Asundi, A., Chen, Q.: High-resolution transport-of-intensity quantitative phase microscopy with annular illumination. Sci. Rep. **7**(1), 1 (2017)